

Searching for axion-like particles under strong gravitational lenses

Aritra Basu^{1,*}, Jishnu Goswami¹, Dominik J. Schwarz¹, and Yuko Urakawa^{1,2}

¹*Fakultät für Physik, Universität Bielefeld, Postfach 100131, 33501 Bielefeld, Germany*

²*Department of Physics and Astrophysics, Nagoya University, Chikusa, Nagoya 464-8602, Japan*

(Dated: October 28, 2021)

We establish strong gravitational lens systems as robust probes of axion-like particles (ALPs) — a candidate for dark matter. A tiny interaction of photons with ALPs induces birefringence. Multiple images of gravitationally lensed polarised objects allow differential birefringence measurement, alleviating systematics and astrophysical dependencies. We apply this novel method to the lens system CLASS B1152+199 and constrain ALP-photon coupling $\leq 9.2 \times 10^{-11} \text{ GeV}^{-1}$ to $7.7 \times 10^{-8} \text{ GeV}^{-1}$ (95% C.L.) for ALP mass between $3.6 \times 10^{-21} \text{ eV}$ and $4.6 \times 10^{-18} \text{ eV}$. A larger sample will improve the constraints.

Introduction.— Gravitational effects revealed that a quarter of the energy in the Universe is contained in *dark matter*. Its nature remains elusive, as it interacts only weakly with visible matter. Various particles beyond the Standard Model have been proposed as dark matter candidates [1]. *Axions* [2, 3] and *axion-like particles* (ALPs) are very promising candidates [4–7]. The allowed mass range for ALPs spans tens of orders of magnitude and massive efforts are underway to search for their signatures through a multitude of approaches [e.g., 8–11].

A promising direction of ALP searches focuses on its parity-violating interaction with photons through the coupling $g_{a\gamma}$, causing the left- and right-handed circular polarisations of light to propagate at different velocities in the ALP field — the *birefringence* phenomenon [12, 13]. Consequently, the plane of polarisation of linearly polarised light is rotated with respect to the plane at emission and the amount of rotation $\Delta\theta_a$ depends on $g_{a\gamma}$. Since the ALP field oscillates in time with period $T_a = 2\pi/m_a$, where m_a denotes the ALP mass, $\Delta\theta_a$ also oscillates and thus allows to measure m_a .

ALP induced birefringence is achromatic and $\Delta\theta_a$ can be measured through observations of suitable linearly polarised astrophysical systems. For example, indirect linear polarisation at a wavelength of $1.6 \mu\text{m}$ caused by scattered light from the parent star in a proto-planetary disk [14], multi-epoch observations at 2 cm of inherently linearly polarised synchrotron emission from knots in parsec-scale jets of active galactic nuclei (AGN) [15], and *E*-mode polarisation of the cosmic microwave background radiation [11, 16] have been used to constrain ultra-light ALPs. Besides birefringence, alternative approaches have also been used, such as, interconversion between photons and ALPs in the presence of background magnetic fields giving rise to modulations of X-ray spectrum of AGN in a cluster [17, 18] and probing gravitational effects of the oscillating ALP field in the pulse time of arrival from pulsars in a pulsar timing array [19, 20].

In this work we establish strong gravitational lens systems with polarised sources as a powerful new probe of ultra-light ALPs via birefringence. Established astrophysical probes of ALPs heavily rely on assumptions and

modelling, or are limited by instrumental offset and sensitivity [11, 14, 15], and are often sensitive to measure either $g_{a\gamma}$ [17] or m_a [20]. Broadly speaking, they address different aspects — do ALPs exist, and, whether they are the dark matter. In this work, we show that spectro-polarimetric observations at GHz-frequencies of strong gravitational lens systems that produce multiple images of a polarised source provide a unique advantage for probing dark matter in the form of ultra-light ALPs. Multiple images from lensing allow for performing differential polarisation angle measurements which alleviates instrumental offsets and does not rely on modelling the intrinsic astrophysics of the system. Differential measurements facilitates firm estimation of m_a and $g_{a\gamma}$.

Differential measurements.— Measuring the birefringence angle is faced with two challenges — (1) accuracy of instrumental polarisation angle calibration, and, (2) additional chromatic birefringence introduced by Faraday rotation when linearly polarised signals traverse through magnetised plasma. Although current instruments are capable of measuring the angle of polarisation to a fraction of a degree, the accuracy of absolute angle measurement is limited to a few degrees due to the accuracy to which the polarisation angle of astronomical calibrators are known. The second challenge, Faraday rotation, depends on the photon frequency ν wherein the plane of polarisation is given as $\theta(\nu) = \theta_0 + \text{RM}(c/\nu)^2$. Here, θ_0 is the angle of the plane of linear polarisation of the polarised source, and, RM is the Faraday rotation measure, the integral of the magnetic field component parallel to the line of sight weighted by free-electron number density. The effects of Faraday rotation are vastly reduced by performing observations at high frequencies ($> 100 \text{ GHz}$). However, at these frequencies very few astrophysical systems give rise to substantial linearly polarised emission.

In most astrophysical sources, linearly polarised emission at few GHz frequencies directly originates from the synchrotron mechanism. However, in these frequencies, Faraday rotation introduces complicated frequency variation of the linear polarisation parameters, Stokes *Q* and *U*, when polarised signal propagates through turbulent magnetised media [21]. These frequency variations are

captured by polarisation measurements performed over large bandwidths, and are robustly modelled by applying the technique of Stokes Q, U fitting. Stokes Q, U fitting enables determination of the Faraday rotation-corrected polarisation angle θ_0 emitted by a source as one of the fitted parameters [22, 23]. Since the birefringence induced by the interaction of photons with ALP field is achromatic, the measured $\theta_0 = \theta_{\text{qso}} + \Delta\theta_a + \delta\theta_{\text{cal}}$. θ_{qso} is the intrinsic polarisation angle of a linearly polarised source, e.g., a quasar, and, $\delta\theta_{\text{cal}}$ is the offset angle due to improper calibrations. For observations of a quasar along a single line of sight, it is unfeasible to determine $\Delta\theta_a$ without the knowledge of θ_{qso} and $\delta\theta_{\text{cal}}$.

Strong gravitational lensing of polarised objects yields a unique advantage in mitigating the unknown θ_{qso} and $\delta\theta_{\text{cal}}$. Gravitational lensing offers the opportunity to simultaneously observe time-separated emission from a source, due to gravitational time delay, as lensed images. The time-separated images encode the time variation of the oscillating ALP field at the emitting source and therefore, the polarisation plane of each lensed images undergo different amount of birefringence. Comparing the polarisation angle of lensed images provide information on $\Delta\theta_a$. Polarised signals which were emitted by the source at initial times t_i with $i = A, B$ for the two images A and B are observed simultaneously at time t_{obs} . The gravitational time delay observed on Earth $\Delta t_{\text{obs}} = |t_A - t_B|(1 + z_{\text{qso}})$, where z_{qso} is the redshift of the lensed quasar. By performing Stokes Q, U fitting separately for each image, the polarisation angles of image A and B, $\theta_{0,A}$ and $\theta_{0,B}$, can be obtained. Both $\theta_{0,A}$ and $\theta_{0,B}$ contain the same θ_{qso} and $\delta\theta_{\text{cal}}$, but different rotation angles, $\Delta\theta_{a,A}$ and $\Delta\theta_{a,B}$, arising from the time separation. Therefore, the differential angle $\Delta\theta_{a,\text{lens}} = \theta_{0,A} - \theta_{0,B} = \Delta\theta_{a,A} - \Delta\theta_{a,B}$ does not depend on θ_{qso} or $\delta\theta_{\text{cal}}$. The significance of the result is determined by statistical measurement noise. The birefringence in a similar setup was considered to explore the anomalous coefficient of axion strings [24] and for detecting cosmic axion background using polarised pulsars [25].

Differential birefringence.— We consider the Lagrangian density for an ALP field a given as,

$$\mathcal{L} = -\frac{1}{4}F_{\mu\nu}F^{\mu\nu} - \frac{1}{2}\partial_\mu a \partial^\mu a + \frac{g_{a\gamma}}{4}aF_{\mu\nu}\tilde{F}^{\mu\nu} - \frac{1}{2}m_a^2 a^2, \quad (1)$$

where $F_{\mu\nu}$ denotes the electromagnetic field strength tensor and $\tilde{F}^{\mu\nu}$ is its dual. We use the Heaviside-Lorentz system with $\hbar = c = 1$. The equation of motion for a is given by the Klein-Gordon equation, solved as,

$$a(t, x^i) = \frac{\sqrt{2\rho_a(x^i)}}{m_a} \sin(m_a t + \delta(x^i)). \quad (2)$$

Here, x^i represents the three spatial coordinates, ρ_a is the energy density of the ALP field, and δ is the phase. Inhomogeneities of the ALP field are encoded in the spatial

dependencies of ρ_a and δ , with δ being constant within patches of size of the de Broglie wavelength λ_{dB} .

The parity-violating coupling term $aF\tilde{F}$ gives rise to birefringence. As the ALP field oscillates, the birefringence angle also oscillates in time. When temporal and spatial variations of the ALP field are much smaller than the frequency of the photons propagating in the ALP field, satisfying $10^{-16}(m/10^{-22} \text{ eV})(\text{GHz}/\nu) \ll 1$, the rotation angle is given as [11, 12, 16, 26],

$$\Delta\theta_a = \frac{1}{2}g_{a\gamma} [a(t_{\text{obs}}, x_{\text{obs}}^i) - a(t_{\text{em}}, x_{\text{em}}^i)]. \quad (3)$$

The subscripts ‘obs’ and ‘em’ indicate the ALP field at observation and at photon emission, respectively. Thus, in order to infer $g_{a\gamma}$, the field values at emission region and at observations has to be known or assumed [15].

For $\Delta\theta_a$ measured towards two gravitationally lensed images A and B, the field $a(t_{\text{obs}}, x_{\text{obs}}^i)$ is the same. In such a case, the differential birefringence angle $\Delta\theta_{a,\text{lens}} = \Delta\theta_{a,A} - \Delta\theta_{a,B}$ depends only on the properties of ALP field in the emitting region and is not affected by the space-time curvature of the gravitational lens [26]. Thus, using Eqs. (2) and (3),

$$\Delta\theta_{a,\text{lens}} = K \sin\left[\frac{m_a \Delta t}{2}\right] \sin(m_a t_{\text{em}} + \delta_{\text{em}} - \pi/2). \quad (4)$$

Here, K in normalized units is,

$$K = 10^\circ \left[\frac{\rho_{a,\text{em}}}{20 \text{ GeV cm}^{-3}} \right]^{1/2} \frac{g_{a\gamma}}{10^{-12} \text{ GeV}^{-1}} \left[\frac{m_a}{10^{-22} \text{ eV}} \right]^{-1}. \quad (5)$$

We have used $\rho_{a,A} = \rho_{a,B} \equiv \rho_{a,\text{em}}$ (the energy density of the ALP field in the emitting region), and, $t_{\text{em}} = (t_A + t_B)/2$ is the mean time of emission. The phase difference δ_{em} is the same for the emitting region. Thus, the amplitude of the differential birefringence signal depends on the lensing time delay measured in the frame of the emitting source, $\Delta t = |t_A - t_B|$. In Eq. (4), the $\sin(m_a t_{\text{em}} + \delta_{\text{em}} - \pi/2)$ term suggests that $\Delta\theta_{a,\text{lens}}$ would also oscillate with the same time period as that of the ALP field determined by m_a , but shifted in phase by 90° . With sufficiently sensitive observations, the oscillation of $\Delta\theta_{a,\text{lens}}$ can be measured through regular monitoring of a lens system and m_a can be measured.

Based on a measurement of $\Delta\theta_{a,\text{lens}}$ at a single epoch, the ratio of the ALP-photon coupling and ALP mass, $g_{a\gamma}/m_a$, can be inferred for a given ρ_a determined through ancillary measurements. This therefore provides $g_{a\gamma}$ over a range of m_a . The time-scales involved in the emission, observations, and light propagation determine the range of ALP masses that can be probed. For a single epoch, $\Delta\theta_{a,\text{lens}}$ is given as, $\Delta\theta_{a,\text{lens}} = K \sin(m_a \Delta t/2)/\sqrt{2}$, where the factor $1/\sqrt{2}$ originates from the root mean square of the oscillating ALP field with a random phase. Note that, in the case when $T_a \gg \Delta t$, the values of the field for image A and B

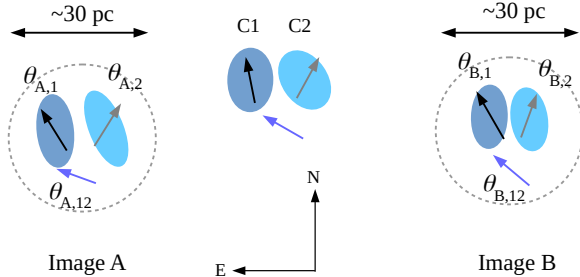


FIG. 1. Schematic of polarisation angle orientations for the two lensed images of the background quasar in CLASS B1152+199. The angles $\theta_{A,i}$ and $\theta_{B,i}$ ($i = 1, 2$, and, 12) are used for our calculations. The presented angles are measured towards East from North of the coordinate axes shown here. The blobs marked as ‘C1’ and ‘C2’ depict the two polarised components. The dashed circles show a schematic spatial resolution of ~ 30 pc at the distance of the quasar. The relative shapes and orientations of the components in the lensed images are different to indicate shearing due to lensing. The extent of shearing of the components and their angles are exaggerated for representation and are not to scale.

would be close to each other and the differential birefringence would be negligible. Therefore, the lensing time delay determines the minimum ALP mass ($m_a = 2\pi/\Delta t$) to which a single epoch observation is sensitive. The maximum ALP mass is determined by the averaging time t_{avg} of observations in the frame of the lensed object. This is because, field oscillations on smaller time-scales due to ALP with $m_a > 2\pi/t_{\text{avg}}$ will be averaged out in the observations.

When a lens system is regularly observed over a period of time $t_{\text{monitor}} \gg \Delta t$, the accessible mass range increases towards lower $m_a = 2\pi/t_{\text{monitor}}$. With sufficiently sensitive observations during the course of the monitoring, the sinusoidal oscillation of $\Delta\theta_{a,\text{lens}}$ should be observed if m_a is smaller than the corresponding time over which data are averaged in each of the observations. In the event of non-detection, limits obtained on $\Delta\theta_{a,\text{lens}}$ could extend the ruled out parameter space for ALPs as compared to that obtainable for a single epoch observation. A long monitoring program corresponds to the limit $m_a \Delta t \ll 1$, and from Eq. (4), $\Delta\theta_{a,\text{lens}}$ can be constrained using the relation $\Delta\theta_{a,\text{lens}} = K m_a \Delta t / 2\sqrt{2}$.

Constraint from CLASS B1152+199.— The lens system CLASS B1152+199 is a highly suitable candidate for probing ALPs and has been studied in detail in the literature providing relevant information. CLASS B1152+199 is a galaxy gravitational lens system wherein a foreground star-forming galaxy at redshift $z_{\text{gal}} = 0.439$ lenses a background linearly polarised quasar at redshift $z_{\text{qso}} = 1.019$ [27, 28]. Using an isothermal sphere mass distribution model for the lensing galaxy, the best-fit time delay Δt_{obs}

TABLE I. Best-fit intrinsic polarisation angle of the polarised emission components in CLASS B1152+199 taken from table 1 of [30].

Image	Component 1	Component 2
A	$\theta_{A,1} = 32^\circ \pm 1^\circ$	$\theta_{A,2} = -38^\circ \pm 4^\circ$
B	$\theta_{B,1} = 30^\circ \pm 10^\circ$	$\theta_{B,2} = -20^\circ \pm 20^\circ$

is estimated to be 27.8 days [28], which corresponds to $\Delta t = 13.3$ day in the frame of the quasar [29].

Broad-band polarisation observations of this system, covering the frequency range 1 to 8 GHz, were performed using the Karl G. Jansky Very Large Array (VLA) to constrain the magnetic field geometry in the lensing galaxy [30]. The background quasar is lensed into two images, denoted by image A and B, separated by 1.56 arcsec. Both images were detected in the VLA observations, and their polarisation spectra were independently fitted using the technique of Stokes Q, U fitting [30]. It was found that the polarised emission of each of the images are composed of two polarisation emitting components which undergo Faraday rotation and depolarisation in the magnetised plasma of the lensing galaxy. These polarised components, denoted as component 1 and 2, remained unresolved in the VLA observations at up to 0.5 arcsec [30]. From milli-arcsec resolution observations [28], these polarised components are physically separated by < 30 pc. The fitted angle of polarisation of each of the polarised components in the lensed images are presented in Table I. We denote the Faraday rotation-corrected angles with corresponding image and component as subscripts, i.e., $\theta_{I,C}$ where $I = A, B$ represents the lensed images and $C = 1, 2$ corresponds to the polarised components. A pictorial representation of the different polarisation angles is shown in Fig. 1.

Presence of multiple polarised emission components in each of the lensed images of the background quasar provides the advantage of measuring three independent angle differences for the two lines of sight, i.e., two angle difference of the individual polarised components $\Delta\theta_1 = \theta_{A,1} - \theta_{B,1}$ and $\Delta\theta_2 = \theta_{A,2} - \theta_{B,2}$, and the difference of relative angles between the two polarised components $\Delta\theta_{12} = (\theta_{A,1} - \theta_{A,2}) - (\theta_{B,1} - \theta_{B,2})$. Each of the angle difference measures $\Delta\theta_{a,\text{lens}}$, and the combined mean provides the net angle difference between the two lines of sight. This follows from the fact that emission from the components within 30 pc is comparable to λ_{dB} for ALP dark matter with $m_a \sim 10^{-20}$ eV and velocity dispersion ~ 100 km s $^{-1}$.

Differential angle measurements do not depend on the choice of the coordinate system, except for the sense in which the difference is calculated. Here, we always measure angle differences with respect to image A. Because of periodicity of angles, we apply directional statistics [31, 32] to compute the mean $\Delta\theta_{a,\text{lens}}$. As there are only three independent measures of birefringence angles,

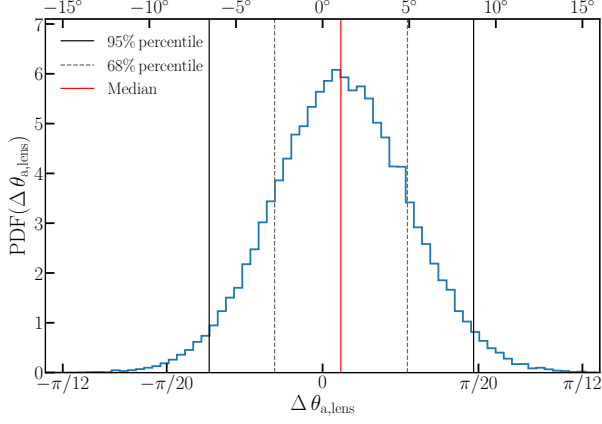


FIG. 2. Distribution of $\Delta\theta_{a,\text{lens}}$ calculated from modified Von Mises distribution of angles presented in Table I. The red line shows the location of the median of the distribution, and the solid and the dashed lines are the 95% and 68% percentile confidence intervals around the median.

$\Delta\theta_1, \Delta\theta_2$ and $\Delta\theta_{12}$, we have performed a Monte-Carlo simulation with 50,000 realizations of $\theta_{A,1}, \theta_{A,2}, \theta_{B,1}$ and $\theta_{B,2}$, each of which is drawn from a modified Von Mises probability distribution function (PDF) of the form,

$$\text{PDF}(\theta) = \frac{1}{I_0(\kappa)} e^{\kappa \cos[2(\theta - \mu)]}, \text{ for } -\frac{\pi}{2} \leq \theta \leq +\frac{\pi}{2}, \quad (6)$$

to account for the fact that measurements of synchrotron polarisation are sensitive to the orientation of the polarisation plane and not the direction. μ is the measured angle, κ is the concentration parameter given by the inverse square of the respective error of the measured angle in Table I expressed in radians, and I_0 is the modified Bessel function of order zero.

Fig. 2 shows the PDF of $\Delta\theta_{a,\text{lens}} = \langle \Delta\theta_i \rangle$, where $i = 1, 2$ and 12, computed using weighted circular mean from random realizations of $\theta_{A,1}, \theta_{A,2}, \theta_{B,1}$ and $\theta_{B,2}$. The inverse of the dispersion ($\sigma_{\Delta\theta_i}$) of $\Delta\theta_1, \Delta\theta_2$ and $\Delta\theta_{12}$ distributions were used as their corresponding weights, $w_i = \sigma_{\Delta\theta_i}$. The distribution of $\Delta\theta_{a,\text{lens}}$ is well represented by a normal distribution. We used the median value of the distribution and obtain $\Delta\theta_{a,\text{lens}} = 1.04^{+3.90}_{-1.80}$ deg (68% confidence interval) and $\Delta\theta_{a,\text{lens}} = 1.04^{+7.67}_{-5.59}$ deg (95% confidence interval). These provide the upper limit $|\Delta\theta_{a,\text{lens}}| < 4.94^\circ$ at 68% confidence level (C.L.) and $< 8.71^\circ$ at 95% C.L. If uniform weighting ($w_i = 1$) is used instead, the bounds on $|\Delta\theta_{a,\text{lens}}|$ improves by about 1° .

A part of $\Delta\theta_{a,\text{lens}}$ could arise due to slight differences of the geodesics along which the polarised light travels for the two lensed images and differential gravitational shearing encountered by the two lensed images. Both these effects are of the order of the lensing deflection angle [33]. For CLASS B1152+199, the deflection angle is 1.56 arcsec, significantly lower than the measured error

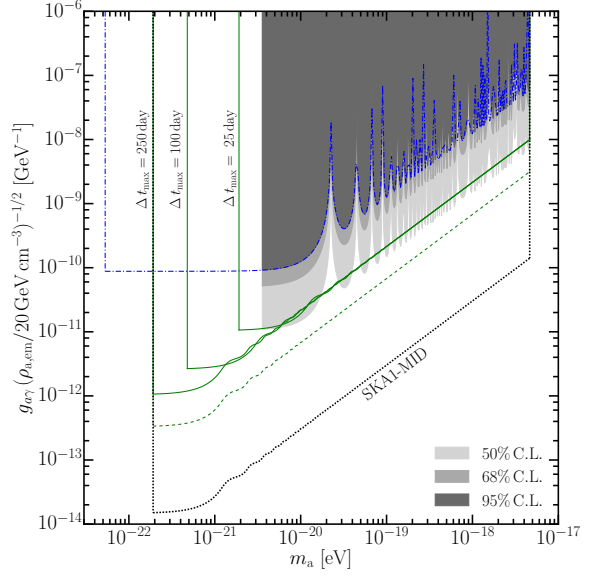


FIG. 3. Bounds on $g_{a\gamma}$ obtained from CLASS B1152+199 is shown as the shaded gray areas. The dash-dotted blue line shows the corresponding constraint that can be achieved if observations of CLASS B1152+199 are sampled over ~ 5 year. The solid and dashed green lines show the constraint achievable for a sample of 100 and 1000 gravitational lens systems, respectively (see text). The various Δt_{max} values for maximum time delay in the frame of the lensed source represent the respective constraints. The dashed green line is for $\Delta t_{\text{max}} = 250$ day. The dotted black line shows the parameter space that can be probed by the SKA1-MID.

for the angle difference between the two images. Hence, the contributions of different light travel paths and shearing in $\Delta\theta_{a,\text{lens}}$ are negligible. Further, the total radio continuum intensity of CLASS B1152+199 at 8.46 GHz was monitored using the VLA spanning over 7 months with an average observation spacing of 3.5 days [34]. No time variability in the intensities of the two lensed images were observed. This strongly suggests that any changes in the polarisation angles between the polarised components of the two lensed images is unlikely to be due to intrinsic time variability of the lensed quasar.

Using the estimated limit on $\Delta\theta_{a,\text{lens}}$, $g_{a\gamma}$ can be constrained using Eq. (4), where $\rho_{a,\text{em}}$ is the only unknown quantity. It can be assumed within informed range when ALPs are the dark matter (see below). For the CLASS B1152+199 system, $\rho_{a,\text{em}} = 20 \text{ GeV cm}^{-3}$ is assumed for the host galaxy of the quasar. A factor of 10 offset in the assumed $\rho_{a,\text{em}}$ would lead to systematic offset by a factor of ~ 3 in the values of $g_{a\gamma}$.

In Fig. 3, we present our constraint $g_{a\gamma} \leq 9.2 \times 10^{-11} (20 \text{ GeV cm}^{-3} / \rho_{a,\text{em}})^{1/2} \text{ GeV}^{-1}$ to $7.7 \times 10^{-8} (20 \text{ GeV cm}^{-3} / \rho_{a,\text{em}})^{1/2} \text{ GeV}^{-1}$ at 95% C.L. for ALP in the mass range $3.6 \times 10^{-21} \text{ eV} \leq m_a \leq 4.6 \times 10^{-18} \text{ eV}$. As discussed earlier, the maximal ALP mass these obser-

vations are sensitive to is determined by the observations averaging time of 30 minute [30], i.e., $t_{\text{avg}} = 14.86$ minute corresponding to $m_a = 4.6 \times 10^{-18}$ eV. The minimal m_a probed is determined by the time difference Δt over which the emission from the lensed images originate. For CLASS B1152+199, $\Delta t = 13.3$ day corresponds to $m_a = 3.6 \times 10^{-21}$ eV.

For a measurement at a single epoch, m_a remains unknown, even if a detection of $\Delta\theta_{a,\text{lens}}$ would be obtained through sensitive follow-up observations of CLASS B1152+199. Until such data are available, the blue dashed-dotted line in Fig. 3 shows the parameter space that can be probed by the CLASS B1152+199 system at 95% C.L. if observations with similar sensitivity as those of the observations used here are sampled over about 5 year (see above).

Statistical sample. — Constraints on $g_{a\gamma}$ probed using gravitational lensing can be vastly improved for a statistical sample. As this method makes minimal assumptions on astrophysical processes, the sample can consist of any type of lensed system where the lensed object is polarised. As the signal is measured via simple differences, $\Delta\theta_{a,\text{lens}}$ computed for individual lens systems can be simply combined to compute the mean differential birefringence angle $\langle |\Delta\theta_{a,\text{lens}}| \rangle$ of a sample of N lens systems and reducing the uncertainty by $\mathcal{O}(1/\sqrt{N})$.

In a sample of lensing systems, the time delay Δt is a random variable and $\langle |\Delta\theta_{a,\text{lens}}| \rangle$ is proportional to $\langle |\sin(m_a \Delta t/2)| \rangle$, because the variables $\rho_{a,\text{em}}$ and Δt are statistically independent. For a random argument of $\sin(m_a t_{\text{em}} + \delta_{\text{em}} - \pi/2)$, the sample average $\langle |\sin(m_a t_{\text{em}} + \delta_{\text{em}} - \pi/2)| \rangle = 2/\pi$. Assuming a uniform PDF for $\Delta t \in [0, \Delta t_{\text{max}}]$, $\langle |\Delta\theta_{a,\text{lens}}| \rangle$ is given by,

$$\begin{aligned} \langle |\Delta\theta_{a,\text{lens}}| \rangle &= \frac{2g_{a\gamma}\sqrt{2\langle\rho_{a,\text{em}}\rangle}}{\pi m_a \Delta t_{\text{max}}} \int_0^{\Delta t_{\text{max}}} \left| \sin\left(\frac{m_a \Delta t}{2}\right) \right| d(\Delta t), \\ &= \frac{4K}{\pi m_a \Delta t_{\text{max}}} (2n + 1 - \cos \zeta). \end{aligned} \quad (7)$$

Here, Δt_{max} is the maximum time delay at the frame of lensed quasars in the sample of gravitational lens systems, $\langle\rho_{a,\text{em}}\rangle$ is the sample mean energy density of the ALP field [35], and K is the same as Eq. (5) except that $\rho_{a,\text{em}}$ is replaced with $\langle\rho_{a,\text{em}}\rangle$. The angle $m_a \Delta t_{\text{max}}/2$ is expressed as $m_a \Delta t_{\text{max}}/2 = n\pi + \zeta$, where $\zeta < \pi$ and $n \in \mathbb{Z}^+$ because $|\sin x|$ has $n\pi$ periodicity.

In a statistical sample, the value of the mean birefringence angle depends on $\langle\rho_{a,\text{em}}\rangle$ which can be inferred from dark matter density measured in elliptical galaxies, which host quasars. The total matter density within the Einstein's radii for a sample of elliptical galaxies have been measured through lensing and stellar kinematics [36, 37]. Considering 50% of the mass in ellipticals is contributed by dark matter [38, 39] and ALPs with $m_a > 10^{-24}$ eV comprises the entire dark matter

[9], we estimate $\langle\rho_{a,\text{em}}\rangle = 25 \text{ GeV cm}^{-3}$ with dispersion 14.5 GeV cm^{-3} . Thus, the constraints on $g_{a\gamma}$ that can be obtained from a sample of gravitational lens systems suffer less systematics as compared to assuming a value of $\rho_{a,\text{em}}$ for a single lens system, which, unless measured for that system, can differ between individual objects.

The solid (dashed) green lines in Fig. 3 show the prediction for a sample of 100 (1000) gravitational lens systems having different values of Δt_{max} in the frame of the lensed object for $\langle\rho_{a,\text{em}}\rangle = 20 \text{ GeV cm}^{-3}$. Due to the large sample size, the sensitivity in measuring the birefringence angle improves by a factor of 10 (32) over the value obtained for CLASS B1152+199. The Phase 1 of the Square Kilometre Array-MID (SKA1-MID) is expected to detect about 10^5 strong gravitational lens systems [40]. Assuming that 5% of the systems will be polarised, we compute the parameter space that can be probed to constrain $g_{a\gamma}$ and is shown by the space above the dotted black line in Fig. 3. For all the expected constraints using different statistical samples, we have extrapolated using the 95% C.L. bound obtained for CLASS B1152+199 and for the SKA1-MID we used a factor of 10 better sensitivity as compared to that of the VLA [41].

Future prospects. — For the ALP mass range probed in this work, the strongest constrain on $g_{a\gamma}$ is obtained using an alternate approach of investigating modulations of the photon spectrum in the X-ray waveband of AGN in a cluster galaxy due to ALP-photon conversion induced by the cluster's magnetic fields [17]. The upper limit $g_{a\gamma} < 1.4 \times 10^{-12} \text{ GeV}^{-1}$ (95% C.L.) depends on astrophysical parameters, such as, structural properties of magnetic fields, free-electron density, and a model of the AGN's X-ray spectrum. The parameter space that can be probed by lensing using the SKA1-MID will improve upon existing bounds on $g_{a\gamma}$ by almost two orders of magnitude for the mass range 10^{-22} to 10^{-20} eV and by up to an order of magnitude in the mass range 10^{-20} to 10^{-19} eV [11, 17].

We have established differential birefringence from strong gravitational lensing as a new robust probe of ultra-light ALPs. In contrast to the existing limit on $g_{a\gamma}$, constraints (and perhaps detection) of ALP from differential birefringence measurements would be independent of astrophysical parameters. Future broad-bandwidth radio polarisation observations of gravitational lensing systems using sensitive radio frequency observations, such as using the SKA or the VLA, will play consequential role in our quest to understand the nature of dark matter.

We thank Pranjal Trivedi, Dietrich Bödeker, Giuseppe Gagliardi, Jordi Miralda Escudé and Anirban Lahiri for insightful discussions on axion physics and ALP birefringence. We acknowledge financial support by the German Federal Ministry of Education and Research (BMBF) under grant 05A17PB1 (Verbundprojekt D-MeerKAT) and from the Deutsche Forschungsgemeinschaft (DFG, German Research Foundation) through the

CRC-TR 211 ‘Strong-interaction matter under extreme conditions’ project number 315477589-TRR 211. Y. U. acknowledges support by JSPS KAKENHI Grant Numbers JP18H04349 and JP19H01894 and in part by YITP-T-19-02.

* Email : aritra@physik.uni-bielefeld.de

- [1] G. Bertone and T. M. P. Tait, *Nature* **562**, 51 (2018), arXiv:1810.01668 [astro-ph.CO].
- [2] R. D. Peccei and H. R. Quinn, *Phys. Rev. Lett.* **38**, 1440 (1977).
- [3] F. Wilczek, *Phys. Rev. Lett.* **40**, 279 (1978).
- [4] J. E. Kim, *Phys. Rev. Lett.* **43**, 103 (1979).
- [5] M. Shifman, A. Vainshtein, and V. Zakharov, *Nucl. Phys. B* **166**, 493 (1980).
- [6] M. Dine, W. Fischler, and M. Srednicki, *Phys. Lett.* **104B**, 199 (1981).
- [7] A. Zhitnitsky, *Sov. J. Nucl. Phys.* **31**, 260 (1980).
- [8] P. W. Graham, I. G. Irastorza, S. K. Lamoreaux, A. Lindner, and K. A. van Bibber, *Annual Review of Nuclear and Particle Science* **65**, 485514 (2015), <https://doi.org/10.1146/annurev-nucl-102014-022120>.
- [9] R. Hlozek, D. Grin, D. J. E. Marsh, and P. G. Ferreira, *Phys. Rev. D* **91**, 103512 (2015), arXiv:1410.2896 [astro-ph.CO].
- [10] I. G. Irastorza and J. Redondo, *Progress in Particle and Nuclear Physics* **102**, 89 (2018).
- [11] G. Sigl and P. Trivedi, arXiv e-prints, arXiv:1811.07873 (2018), arXiv:1811.07873 [astro-ph.CO].
- [12] D. Harari and P. Sikivie, *Phys. Lett.* **B289**, 67 (1992).
- [13] S. M. Carroll, *Phys. Rev. Lett.* **81**, 3067 (1998), arXiv:astro-ph/9806099.
- [14] T. Fujita, R. Tazaki, and K. Toma, *Phys. Rev. Lett.* **122**, 191101 (2019), arXiv:1811.03525 [astro-ph.CO].
- [15] M. M. Ivanov, Y. Y. Kovalev, M. L. Lister, A. G. Panin, A. B. Pushkarev, T. Savolainen, and S. V. Troitsky, *JCAP* **2019**, 059 (2019), arXiv:1811.10997 [astro-ph.CO].
- [16] M. A. Fedderke, P. W. Graham, and S. Rajendran, *Phys. Rev. D* **100**, 015040 (2019), arXiv:1903.02666 [astro-ph.CO].
- [17] M. Berg, J. P. Conlon, F. Day, N. Jennings, S. Krippendorff, A. J. Powell, and M. Rummel, *Astrophys. J.* **847**, 101 (2017), arXiv:1605.01043 [astro-ph.HE].
- [18] A. Ayad and G. Beck, arXiv e-prints, arXiv:1911.10078 (2019), arXiv:1911.10078 [astro-ph.HE].
- [19] A. Khmelnitsky and V. Rubakov, *JCAP* **1402**, 019 (2014), arXiv:1309.5888 [astro-ph.CO].
- [20] N. K. Porayko *et al.*, *Phys. Rev. D* **98**, 102002 (2018), arXiv:1810.03227 [astro-ph.CO].
- [21] D. Sokoloff, A. Bykov, A. Shukurov, E. Berkhuijsen, R. Beck, and A. Poezd, *Mon. Not. R. Astron. Soc.* **299**, 189 (1998).
- [22] S. O’Sullivan, S. Brown, T. Robshaw, D. Schnitzeler, N. McClure-Griffiths, I. Feain, A. Taylor, B. Gaensler, T. Landecker, L. Harvey-Smith, and E. Carretti, *Mon. Not. R. Astron. Soc.* **421**, 3300 (2012), arXiv:1201.3161.
- [23] S. P. O’Sullivan, C. R. Purcell, C. S. Anderson, J. S. Farnes, X. H. Sun, and B. M. Gaensler, *Mon. Not. R. Astron. Soc.* **469**, 4034 (2017), arXiv:1705.00102 [astro-ph.GA].
- [24] P. Agrawal, A. Hook, and J. Huang, (2019), arXiv:1912.02823 [astro-ph.CO].
- [25] T. Liu, G. Smoot, and Y. Zhao, *Phys. Rev. D* **101**, 063012 (2020), arXiv:1901.10981 [astro-ph.CO].
- [26] D. J. Schwarz, J. Goswami, and A. Basu, arXiv e-prints, arXiv:2003.10205 (2020), arXiv:2003.10205 [hep-ph].
- [27] S. T. Myers, D. Rusin, C. D. Fassnacht, R. D. Blandford, T. J. Pearson, A. C. S. Readhead, N. Jackson, I. W. A. Browne, D. R. Marlow, P. N. Wilkinson, L. V. E. Koopmans, and A. G. de Bruyn, *Astron. J.* **117**, 2565 (1999), arXiv:astro-ph/9905043 [astro-ph].
- [28] D. Rusin, M. Norbury, A. D. Biggs, D. R. Marlow, N. J. Jackson, I. W. A. Browne, P. N. Wilkinson, and S. T. Myers, *Mon. Not. R. Astron. Soc.* **330**, 205 (2002), astro-ph/0110099.
- [29] Note that, [28] computed $\Delta t_{\text{obs}} = 39.7$ day for the assumed Hubble-Lemaître constant $H_0 = 100 \text{ km s}^{-1} \text{ Mpc}^{-1}$. Here, we have corrected the estimated time delay using $H_0 = 67.4 \text{ km s}^{-1} \text{ Mpc}^{-1}$ obtained from the *Planck* satellite’s data [42] and used $\Delta t_{\text{obs}} = 27.8$ day in our calculations.
- [30] S. A. Mao, C. Carilli, B. M. Gaensler, O. Wucknitz, C. Keeton, A. Basu, R. Beck, P. P. Kronberg, and E. Zweibel, *Nature Astronomy* **1**, 621 (2017).
- [31] N. Fisher, *Statistical Analysis of Circular Data*, Cambridge: Cambridge University Press (1993).
- [32] K. V. Mardia, P. E. Jupp, (2000), *Directional Statistics*, John Wiley & Sons, Inc., New York (2000).
- [33] M. Lyutikov, *Phys. Rev. D* **95**, 124003 (2017), arXiv:1703.00601 [gr-qc].
- [34] N. Rumbaugh, C. D. Fassnacht, J. P. McKean, L. V. E. Koopmans, M. W. Auger, and S. H. Suyu, *Mon. Not. R. Astron. Soc.* **450**, 1042 (2015), arXiv:1410.6557 [astro-ph.CO].
- [35] Here we have made the approximation $\langle \rho_{a,\text{em}}^{1/2} \rangle \approx \langle \rho_{a,\text{em}} \rangle^{1/2}$. This is valid when $\langle \rho_{a,\text{em}} \rangle$ is larger than the dispersion of $\rho_{a,\text{em}}$.
- [36] L. V. E. Koopmans, T. Treu, A. S. Bolton, S. Burles, and L. A. Moustakas, *Astroph. J.* **649**, 599 (2006), arXiv:astro-ph/0601628 [astro-ph].
- [37] N. Lyskova, E. Churazov, and T. Naab, *Mon. Not. R. Astron. Soc.* **475**, 2403 (2018), arXiv:1711.01123 [astro-ph.GA].
- [38] N. Lyskova, E. Churazov, A. Moiseev, O. Sil’chenko, and I. Zhuravleva, *Mon. Not. R. Astron. Soc.* **441**, 2013 (2014), arXiv:1404.2729 [astro-ph.GA].
- [39] M. R. Lovell, A. Pillepich, S. Genel, D. Nelson, V. Springel, R. Pakmor, F. Marinacci, R. Weinberger, P. Torrey, M. Vogelsberger, A. Alabi, and L. Hernquist, *Mon. Not. R. Astron. Soc.* **481**, 1950 (2018), arXiv:1801.10170 [astro-ph.GA].
- [40] J. McKean, N. Jackson, S. Vegetti, M. Rybak, S. Serjeant, L. V. E. Koopmans, R. B. Metcalf, C. Fassnacht, P. J. Marshall, and M. Pandey-Pommier, in *Advancing Astrophysics with the Square Kilometre Array (AASKA14)* (2015) p. 84, arXiv:1502.03362 [astro-ph.GA].
- [41] R. Braun, *et al.*, SKA document number SKA-TEL-SKO-0000818, (2017), https://astronomers.skatelescope.org/wp-content/uploads/2017/10/SKA-TEL-SKO-0000818-01_SKA1_Science_Perform.pdf.
- [42] Planck Collaboration VI, (2018) arXiv:1807.06209.